



Article

The Synthesis of Sn-Containing Silicates Coated with Binaphthol and Their Specific Application for Catalytic Synthesis of 6-Hydroxyhexanoic Acid and Cyclohexylformate through Baeyer-Villiger Oxidation

Jinyi Ma¹, Aqun Zheng¹, Qin Pan^{1,2,*}, Yong Wu^{1,2}, Xiangdong Wang^{1,2}, Xiaoyong Li^{1,2}, Wanqin Wang^{1,2}, Min Gao^{1,2} and Yang Sun^{1,2,*}

¹ Department of Applied Chemistry, School of Chemistry, Xi'an Jiaotong University, No. 28, Xianning West Road, Xi'an 710049, China

² Xixian New District Xingyi Advanced Materials Technology Co., Ltd., Room 1046, 1st floor, Hongdelou, Building No. 20, Science and Technology Innovation Port, Western China, Fengxi New City, Xixian New District, Xi'an 712000, China

* Correspondence: panqin202212@163.com (Q.P.); sunyang79@mail.xjtu.edu.cn (Y.S.); Tel.: +86-(29)-82663914 (Y.S.); Fax: +86-(29)-82668559 (Y.S.)

Abstract: The Baeyer–Villiger oxidation (BVO) of ketone and aldehyde can produce ester and formate, which both have wide applications in many areas. In this work, a series of Sn-containing silicates were prepared through the sol-gel process by using structure-directing and crystallizing agents and post-synthetic coordinated modification of binaphthol. Characterizations revealed that loading of (*L*)-sodium lactate as the crystallizing agent decreased the crystal size of the synthesized catalyst, and there were SnO₂ nanoparticles with sizes of 17–19 nm on the catalyst. Furthermore, quite differently from the 3D mesoporous structure of classical Sn-beta zeolites, the synthesized catalysts had a silt-like mesoporous structure. In the catalysis, when cyclic aliphatic ketones were used as the substrate, only BVO-type products and corresponding ring-opening products were obtained. BVO of aliphatic aldehyde produced both an aerobic oxidation product (carboxylic acid) and a BVO-type product. The presented transformation of aromatic aldehyde (benzaldehyde) only gave an aerobic oxidation product (benzoic acid). The post-synthetic coordinating attachment of (*S*)-binaphthol to the Sn-containing silicate backbone worsened the BVO of aliphatic ketones but improved the BVO of aliphatic aldehyde and the aerobic oxidation of aromatic aldehyde. In addition, this work also developed two new routes for the synthesis of high-value-added 6-hydroxyhexanoic acid and cyclohexylformate under catalytic BVO conditions.

Keywords: Baeyer–Villiger oxidation; Sn-containing silicate; sol-gel synthesis; 6-hydroxyhexanoic acid; cyclohexylformate



Citation: Ma, J.; Zheng, A.; Pan, Q.; Wu, Y.; Wang, X.; Li, X.; Wang, W.; Gao, M.; Sun, Y. The Synthesis of Sn-Containing Silicates Coated with Binaphthol and Their Specific Application for Catalytic Synthesis of 6-Hydroxyhexanoic Acid and Cyclohexylformate through Baeyer-Villiger Oxidation. *Catalysts* **2023**, *13*, 805. <https://doi.org/10.3390/catal13050805>

Academic Editor: Piotr Kuśtrowski

Received: 15 February 2023

Revised: 21 April 2023

Accepted: 24 April 2023

Published: 27 April 2023



Copyright: © 2023 by the authors. Licensee MDPI, Basel, Switzerland. This article is an open access article distributed under the terms and conditions of the Creative Commons Attribution (CC BY) license (<https://creativecommons.org/licenses/by/4.0/>).

1. Introduction

The Baeyer–Villiger oxidation (BVO) of carbonyl substrates, such as ketone and aldehyde, can produce ester (or lactone) and formate, respectively [1], demonstrating high value for the synthesis of biologically important molecules [2] and the manufacture of functional polymers [3] and already standing as a model organic transformation for more than 100 years [1]. Traditional BVO reactions are carried out by using stoichiometric or excessive peracids as the terminal oxidant, such as *m*-chloroperoxybenzoic acid (*m*-CPBA) [4] and peroxybenzoic acid [5]. The mechanism of BVO has been summarized as follows: the nucleophilic attack of the peracid (oxygen atom) against the carbonyl of the substrate first leads to hemiperacetal (Criegee intermediate, Figure 1), which is further degraded to one molecular ester (or lactone) and one molecular carboxylic acid (by-product) through rearrangement (Figure 1) [6]. Migration (rearrangement) of the two substituents

of an unsymmetrical ketone (R and R', Figure 1) would certainly give different products, and the selectivity obtained depends on the migratory aptitude of the two different R groups [6]. Empirically, the substituent that can form a more stable cation usually shows a higher migratory aptitude [6], which is beneficial for the design of substrates to obtain the preferred products.

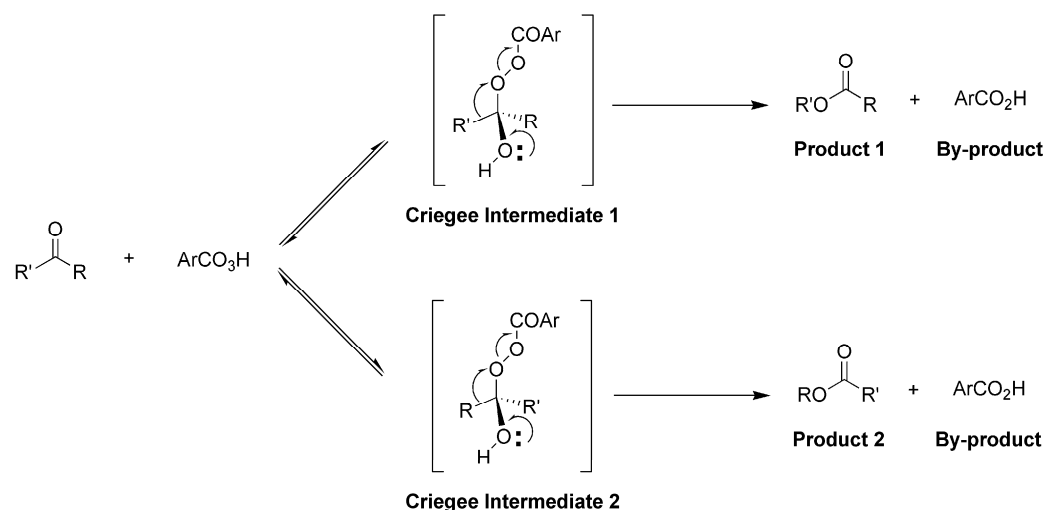


Figure 1. Formation of Criegee intermediate during BVO and origin of migratory aptitude.

Although many esters and formates have been prepared through BVO by employing peracids as the terminal oxidant, most peracids used in BVO are shock-sensitive and produce equimolar unrecyclable carboxylic acids (by-product, Figure 1) [6,7]. Secondly, quite a few peracids show very low BVO yields in the conversion of carbonyl substrates with C=C bonds because they facilitate epoxidation more than BVO [8]. Next, some other traditional BVO processes use stoichiometric and excessive persulfates as the terminal oxidant, but they often need catalysts with strong acidity to accelerate reactions. For example, in the early years, the BVO of simple linear ketones, such as menthone, demanded the combinational use of persulfate with concentrated sulfuric acid for satisfactory conversion [9], but this method is hazardous to the environment.

With the development in this field, catalytic BVO employing environmentally benign oxidants, such as H_2O_2 and O_2 , has come into sight in order to overcome the abovementioned drawbacks. With H_2O_2 as the oxidant, homogeneous catalysts, including Mo [10] and Re [11] complexes, have been developed, indicating that their Lewis and Brønsted acidities can contribute to the formation of the Criegee intermediate (Figure 1). However, these catalysts suffer from poor activity, low lactone selectivity [11], and high costs [10,11]. Moreover, peptide-based catalysts have also been put forward for the BVO of chiral ketones, providing high enantioselectivity and migratory aptitude, but the catalyst cost and product purification are still predicaments for wide application [12].

In order to further improve environmental endurance and decrease production waste, O_2 has been introduced as a new terminal oxidant. For example, the BVO of ketones using O_2 as the sole oxidant in the presence of anilines produced amides when *p*-toluenesulfonic acid (TfOH) was used as a catalyst, but only low to moderate yields were obtained [13], mainly because the acidity of TfOH was not high enough to activate O_2 . Other catalysts, such as metal [14] and enzymes [15], have shown similar tendencies in BVO.

Among the BVO catalysts developed so far, solid acids appear to be highly promising candidates now that the application of H_2O_2 and O_2 has become more available because not only the carbonyl of the substrate but also the inert terminal oxidant can be activated over the porous structure of solid acids [16]. A highly chemoselective and active example is the application of Sn-zeolite beta catalysts first established by Corma and co-workers [17]. In practice, incorporation of Sn^{4+} into the framework of zeolite beta through sol-gel produced

a series of highly efficient catalysts for the BVO of cyclic ketones into lactones with H_2O_2 as the oxidant [17]. Actually, the Sn^{4+} ions being immobilized and highly dispersed into zeolite beta created active Lewis acid centers for the activating carbonyl groups [17]. Furthermore, Sn^{4+} does not promote the epoxidation of the C=C bond on certain carbonyl substrates when using terminal oxidants, such as H_2O_2 , compared to Ti^{4+} , Fe^{3+} , or Cu^{2+} ; thus, formation of disfavored epoxide or other oxide by-products can be avoided, eventually leading to high chemoselectivity [17,18].

However, the large-scale application of Sn-zeolite beta catalysts has encountered two serious obstacles: the long time required for crystallization during synthesis (20 days) and the employment of a fluoride template (using hydrofluoric acid as the medium) [17]. The lengthy synthesis time means slow crystal growth in the Sn-zeolite beta zeolites during the sol-gel synthesis, probably due to the much larger radius of Sn^{4+} (0.71 Å) than that of Si^{4+} (0.41 Å) [19]. The hydrofluoric acid introduced in sol-gel may play a role as a mineralizer to accelerate crystallization [20]. In order to overcome these drawbacks, Zhang and co-workers developed a steam-assisted conversion (SAC) process for the synthesis of Sn-beta zeolites from stannosilicate dry gel, and the total synthesis time was reduced to 20 h [20]. The synthesized Sn-beta zeolite catalysts showed very high lactone selectivities (close to 100%) in catalytic BVO [20]. However, this method still used ammonium fluoride as the mineralizer [20]. Later, fluoride-free synthesis of Sn-BEA catalysts through dry-gel conversion was realized by adding seed crystals [21].

However, due to the fact that Sn^{4+} has a much larger radius than Si^{4+} [19] and direct sol-gel synthesis actually has limited incorporation efficiency for Sn^{4+} [19], post-synthetic methods have been explored to incorporate Sn^{4+} into the defects of some of the denser Sn-containing zeolites, such as Y [22] or FAU ones [23]. These methods involve post-synthetic removal of heteroatoms (Al or B) from the zeolite framework (acid washing), leaving more defects or cavities to accommodate Sn^{4+} [22,23], which has allowed new insights into the synthesis of Sn-containing zeolite catalysts.

Additionally, to promote the permeability of the reactant into the solid catalyst, supercritical CO_2 has been employed as a solvent instead of the frequently used *n*-hexane, and much better conversion was achieved [24]. All in all, the application of Sn-containing zeolites as catalysts seems to be a highly practicable method for establishing highly chemoselective and eco-friendly BVO reactions, but the synthesis of the catalyst, the substrate scope, and the reaction optimization require more work.

It is also interesting and significant to study new products derived from BVO. For example, cyclohexanone (CHONE) can be transformed into ϵ -caprolactone (ϵ -CL) through classical BVO reactions catalyzed by many suitable catalysts [25], but ϵ -CL seems to be more of a useful intermediate than a high-value-added product (Figure 2) [26]. Actually, 6-hydroxyhexanoic acid (HHA), the acid hydrolysate of ϵ -CL, has turned out to be a highly valuable molecule with wide applications in many fields, including in the dermatopharmaceuticals, cosmetics, and polymer industries [26]. In particular, HHA plays a role as a key raw material in the production of polycaprolactone (PCL), which is a biomedical biodegradable polymer with great market demand [27].

However, in practice, the traditional production of HHA appears to be through metal-catalyzed reduction of adipic acid (AA) at 523 K with 300 bar H_2 [28], but this method has a potential risk of explosion, as well as high costs for raw materials and catalysts (Figure 2). Alternatively, a hollow titanium molecular silicate sieve (HTS) produced from TS-1 has often been used as a catalyst for direct BVO-type transformation of CHONE to HHA, but the product is a mixture containing ϵ -CL, HHA, AA, and hydroxyketone, leading to difficulties in product separation [29]. Undoubtedly, there is still room for developing the direct conversion of CHONE into HHA (Figure 2).

In contrast to the BVO of ketones, conversion of aldehydes seems to be less effective, and significant BVO-type products (such as formate) are often found in the transformation of benzaldehyde (Dakin oxidation) [30]. In practice, transformation of most other aldehydes under BVO conditions usually produces carboxylic acids [31]. However, the

BVO conversion of aliphatic aldehydes still deserves attention due to their great synthetic significance. For example, cyclohexylformate was recently developed as a key intermediate for convenient synthesis of cyclohexanol [32], which is a platform molecule for producing adipic acid, caprolactam, hexamethylene diamine, and other fine chemicals [33]. Therefore, it would be interesting to test the synthesis of cyclohexylformate by using BVO conversion of cyclohexanecarbaldehyde.

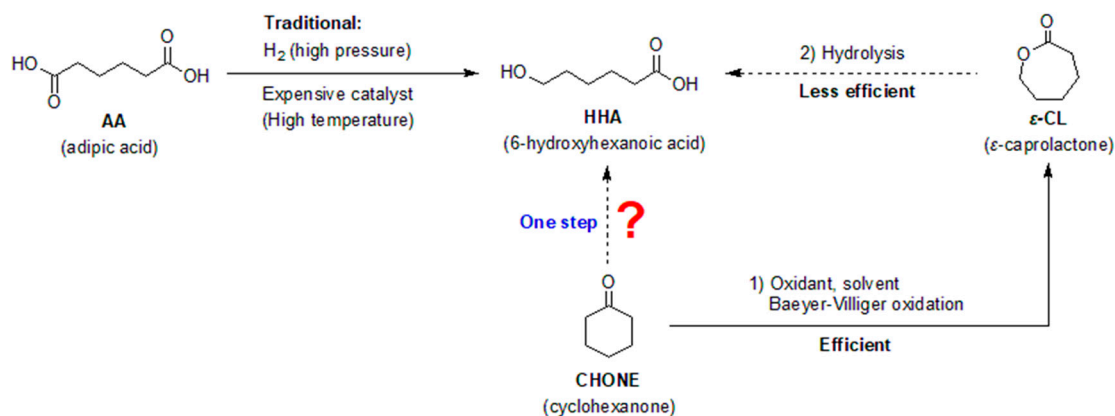


Figure 2. Traditional synthesis of 6-hydroxyhexanoic acid and its preparative challenges.

In this work, a series of Sn-containing silicates were prepared through a sol-gel process, with tin(II) chloride being employed as the Sn precursor, tetraethoxysilane (TEOS) as the Si precursor, hexadecyltrimethylammonium bromide (CTAB) as the structure-directing agent, and sodium lactate as the crystallization reagent. Furthermore, taking into account the fact that the synthesized samples could have Sn components on the surfaces, it was interesting to test the coordination effects of the attached ligands, which probably affect the efficiency of BVO. Therefore, binaphthol was introduced through a post-synthetic procedure. In comparison with the known Sn-containing silicate BVO catalysts, the presented system used a fundamentally different Sn precursor, structure-directing agent, and crystallization reagent, as well as an additional coordinating ligand, which probably led to quite different catalytic outputs, and the system may show potential for future large-scale applications.

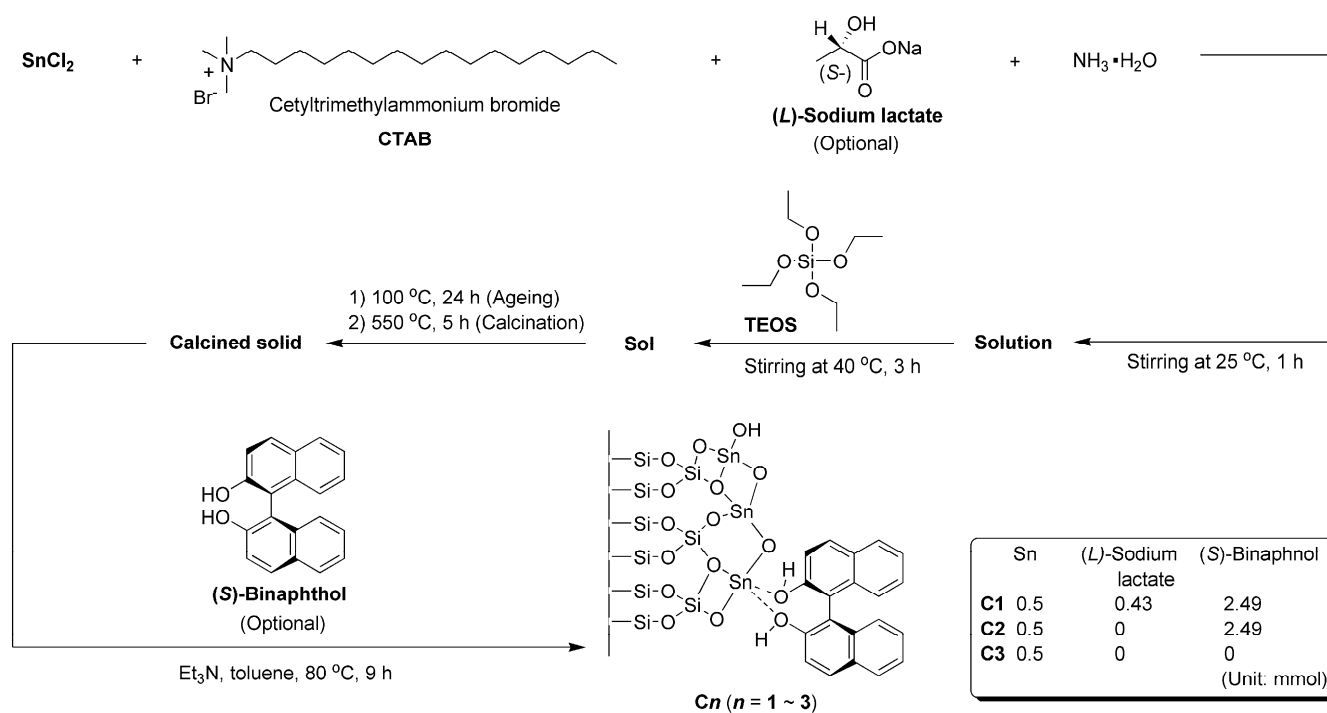
2. Results and Discussion

2.1. Synthesis of Sn-Containing Silicate Catalysts Coated with Binaphthol

As shown in Scheme 1, the Sn-containing silicate catalysts were prepared through a sol-gel process by using tin(II) chloride as the Sn source, tetraethoxysilane (TEOS) as the Si precursor, hexadecyltrimethylammonium bromide (CTAB) as the structure-directing agent, and sodium lactate as the crystallization reagent. Herein, Sn^{2+} was first hydrolyzed to hydroxide in the presence of $NH_3 \cdot H_2O$ and then dehydrated to oxide through ageing and calcination [17]. The resulting calcined solid appeared to be a Sn-Si mixed oxide, the surface Sn centers of which could be further coordinated by binaphthol (Scheme 1).

2.2. Chemical State and Elemental Composition of Catalyst

The chemical state and elemental composition of the catalyst were detected via X-ray photoelectron spectroscopy (XPS), aiming to describe the catalyst surface (depth of 0–3 nm). The XPS survey scan is summarized in Figure 3, while the binding energy and atomic composition are in Table 1. First of all, C1 showed higher C, Si, and Sn content and lower O content than C2 (Table 1), probably indicating that addition of (*L*)-sodium lactate increased the incorporation efficiency of Sn through sol-gel synthesis (Scheme 1). The content of O for C2 was higher than that for C3, while that of Si for C2 was comparatively lower (Table 1), indicating that C2 was coated with (*S*)-binaphthol, in contrast to C3 (Scheme 1).



Scheme 1. Synthesis of Sn-containing silicate catalysts coated with binaphthol.

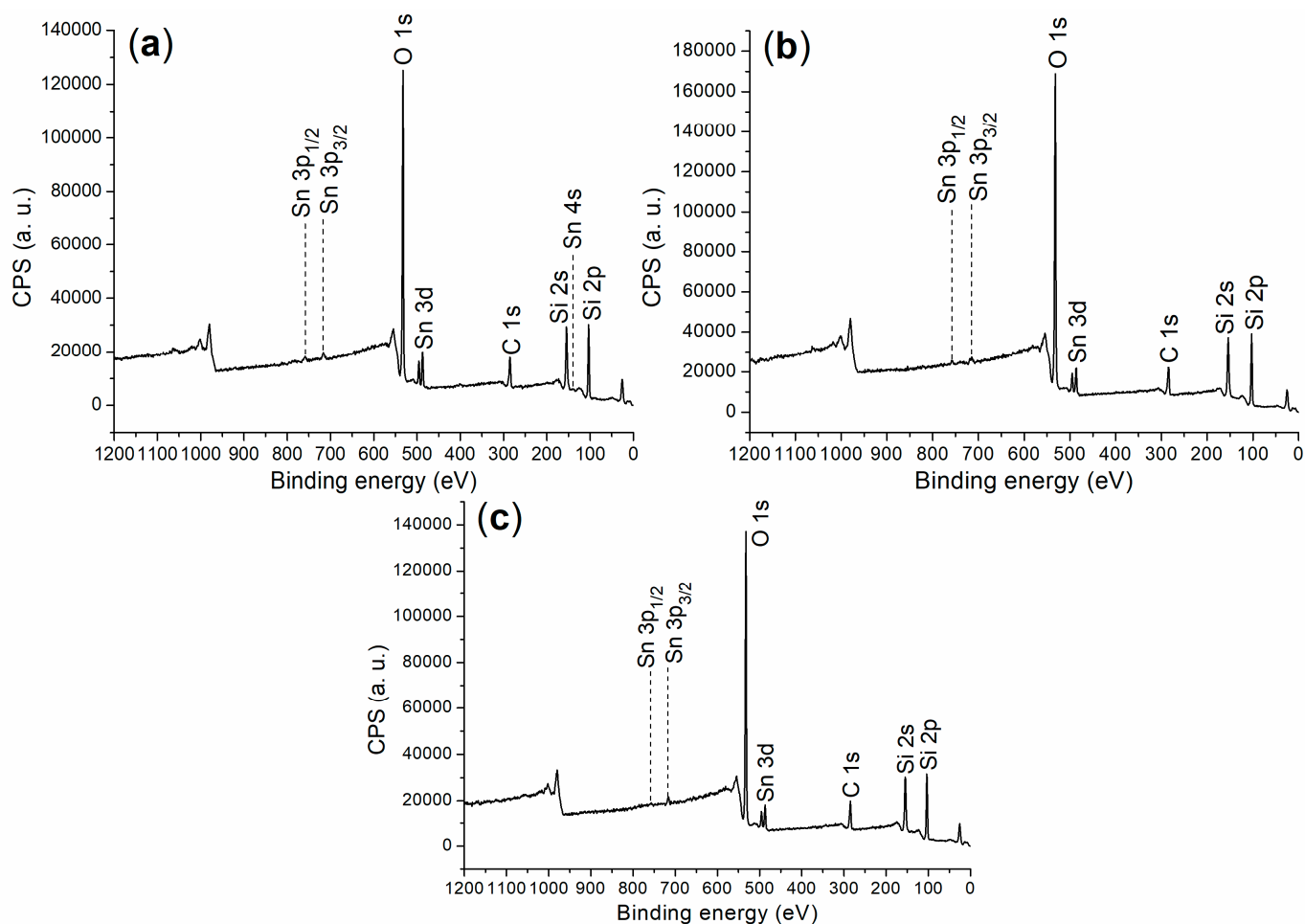


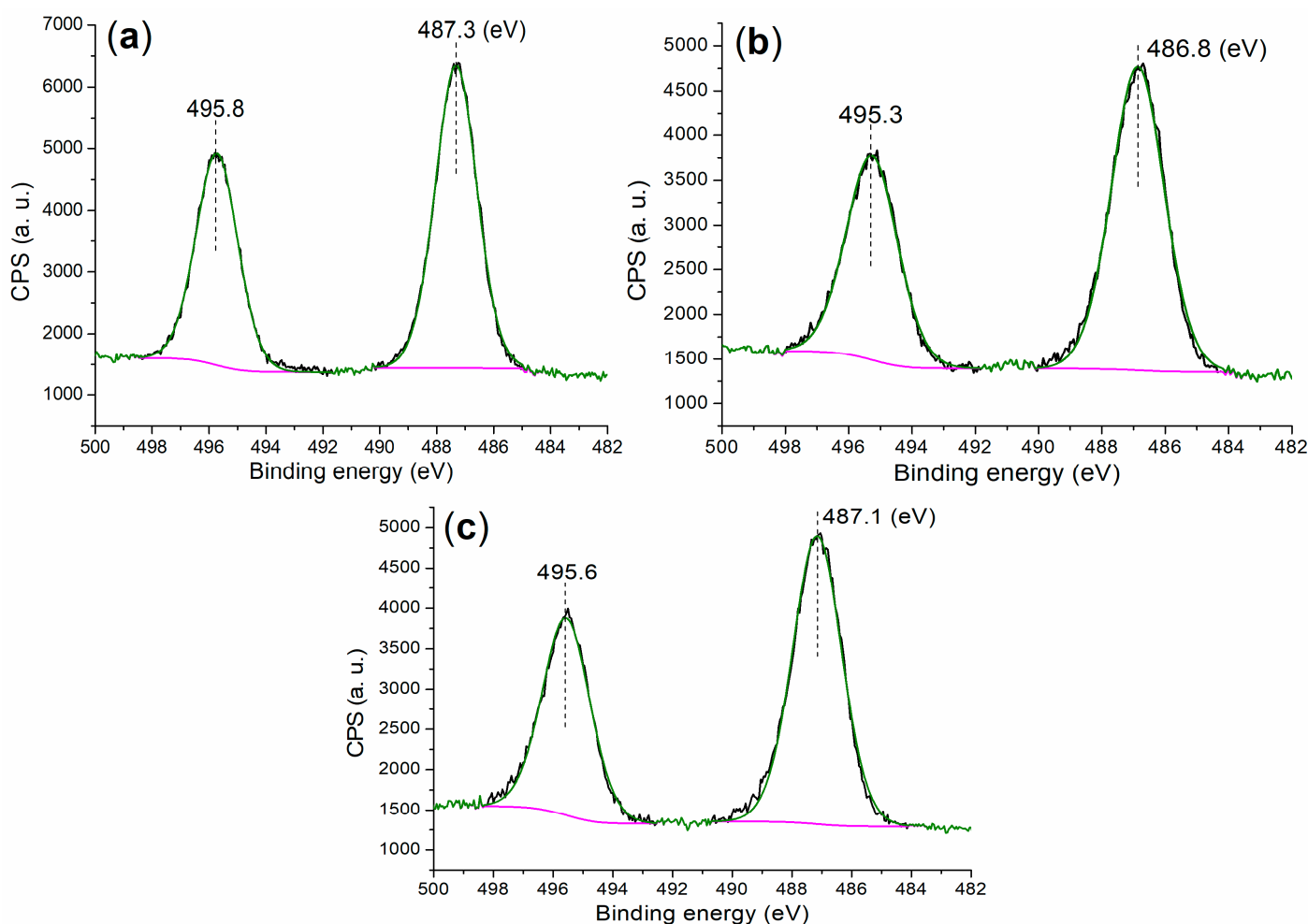
Figure 3. The XPS survey scan for the synthesized catalysts: (a) C1, (b) C2, (c) C3.

Table 1. Binding energy and atomic composition of element on catalyst surface.

Sample	C (1s)	O (1s)	Si (2p)	Sn (3d)
C1	284.80 (14.63) ^a	532.80 (50.26)	103.80 (34.52)	486.80 (0.59)
C2	283.80 (13.95)	531.80 (52.86)	102.80 (32.78)	485.80 (0.40)
C3	284.80 (14.80)	532.80 (50.03)	103.80 (34.77)	486.80 (0.40)

^a Binding energy (eV) with atomic percentage (at%) in parentheses.

It is interesting to discuss the chemical state of the element on the catalyst surface, which is important to understanding the catalytic microenvironment. The Sn 3d regions of the synthesized catalysts are summarized in Figure 4. C1 showed two peaks at 495.8 eV and 487.3 eV (Figure 4a), representing the binding energies of Sn 3d_{3/2} and 3d_{5/2} photoelectrons, respectively, characteristic of Sn⁴⁺ fixed in the SnO₂ phase [34]. In comparison, it has been reported that the binding energy of the Sn 3d_{5/2} photoelectron of Sn²⁺ was located at 485.8 eV and that of metallic Sn at around 485.3 eV [35]. Therefore, although divalent Sn (SnCl₂) was employed as starting material (Scheme 1), the Sn of the synthesized catalyst turned out to be tetravalent. Both C2 and C3 showed similar Sn 3d regions compared to C1 (Figure 4b,c vs. Figure 4a), indicating that C2 and C3 contained Sn⁴⁺ instead of Sn²⁺. Moreover, X-ray diffraction (XRD) was also used to determine the crystallinity of the Sn-containing phase on the catalyst. All the synthesized catalysts (C1–C3) showed diffractions of SnO₂ (cassiterite, PDF No. 41-1445) in the wide-angle XRD (Figure 5a,c), proving the tetravalence of Sn again.

**Figure 4.** XPS measurement of Sn 3d region for synthesized catalysts: (a) C1, (b) C2, (c) C3.

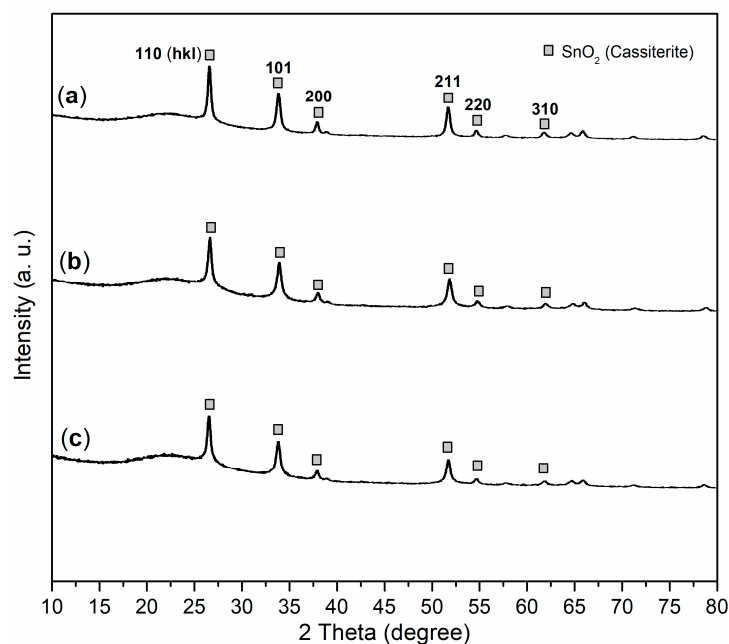


Figure 5. Wide-angle XRD patterns for powdered synthetic catalysts: (a) C1, (b) C2, (c) C3.

In addition, as shown in Figure 6a, there were three components in the C 1s region of C1 occurring at 285.0, 286.4, and 288.9 eV, which are indicative of saturated hydrocarbon (sp^3 hybridization), C-O bonds, and the carboxyl group, respectively [36]. These carbon species may come from organic residues that underwent calcination during the sol-gel process or from the organic ligands attached during the post-synthetic modification (Scheme 1). Other catalysts including C2–C3 also showed three components with similar binding energies and intensities in the C 1s regions (Figure 6b,c vs. Figure 6a), suggesting the same chemical states and distributions of carbon species on the catalyst surface.

2.3. Textural and Other Physical Properties of Catalysts

First of all, all catalysts showed nitrogen physisorption isotherms with similar shapes, with high-pressure sections ($P/P_0 = 0.3-1$) conforming to the type I isotherm and low-pressure sections ($P/P_0 = 0-0.3$) to type II (Figure 7a1,b1,c1), suggesting mesoporous structures (Figure 7a2,b2,c2) [37]. No hysteresis loops were found in these isotherms (Figure 7a1,b1,c1), indicating that all mesopores had silt-like shapes [37]. Furthermore, all catalysts had BET surface areas larger than $400 \text{ m}^2 \text{ g}^{-1}$ (Table 2), suggesting an available approach for the substrate to the internal catalytic centers.

Table 2. Textural properties of synthesized catalysts.

Catalyst	$S_{\text{BET}} (\text{m}^2 \text{ g}^{-1})^a$	$PV (\text{cm}^3 \text{ g}^{-1})^b$	$PR (\text{nm})^c$	$\rho (\text{g cm}^{-3})^d$	$d_{\text{BET}} (\text{nm})^e$
C1	493	0.40	3.12	0.173	70
C2	513	0.42	3.16	0.181	64
C3	460	0.38	3.13	0.175	74

^a Surface area determined by BET method based on N_2 adsorption. ^b BJH adsorption cumulative volume of pores with radii of 1.7–300 nm. ^c Pore radius, BJH method based on N_2 adsorption. ^d Bulk density. ^e Crystallite size based on BET surface area: $d_s = 6 / (S_{\text{BET}} \cdot \rho)$, ρ bulk density [38].

On the other hand, C1 showed a higher amount of acid than C2 (Table 3), indicating that the loading of (*L*)-sodium lactate increased the acidity of the silicate catalyst (Scheme 1). Furthermore, C3 showed a much higher amount of acid than both C1 and C2 (Table 3), clearly indicating that the attachment of (*S*)-binaphthol decreased the acidity due to the coordination of (*S*)-binaphthol with the Sn center on the catalyst surface, and this downward

trend exceeded the upward tendency resulting from the introduction of (*L*)-sodium lactate in the sol-gel process (C1 vs. C2 in Table 3 and Scheme 1).

Table 3. Physical and submicroscopic properties of synthesized catalysts.

Catalyst	Acid Amount	d_{XRD}	d_{W}	ζ_{W}	d_{O}
	(mmol g ⁻¹) ^a	(nm, SnO ₂) ^b	(nm) ^c	(mV) ^d	(nm) ^e
C1	4.3×10^{-4}	19	2698	−194	340
C2	1.7×10^{-4}	17	2871	−186	253
C3	7.0×10^{-3}	17	1899	−83	295

^a Determined by *n*-butylamine titration (Section 3.2). ^b Particle (SnO₂) diameter determined from XRD observations according to Scherrer's equation [39] using 110 diffraction of the SnO₂ component for C1 (Figure 5a), C2 (Figure 5b), and C3 (Figure 5c). ^c Aqueous particle size. ^d Zeta potential of particle in aqueous solution. ^e Size of particle in absolute ethanol.

It was also important to study the size of the SnO₂ particles fixed in the synthesized catalyst. C1 had larger SnO₂ particles than C2 and C3 (d_{XRD} , Table 3), showing that introduction of (*L*)-sodium lactate as a crystallization reagent in the sol-gel process increased the size of SnO₂ (Scheme 1). On the other hand, both C1 and C2 showed much larger hydrated particle sizes than C3 (d_{W} , Table 3), but both C1 and C2 had lower zeta potentials than C3 in water (ζ_{W} , Table 3), indicating that attachment of (*S*)-binaphthol improved the hydrated particle size but decreased stability (Scheme 1).

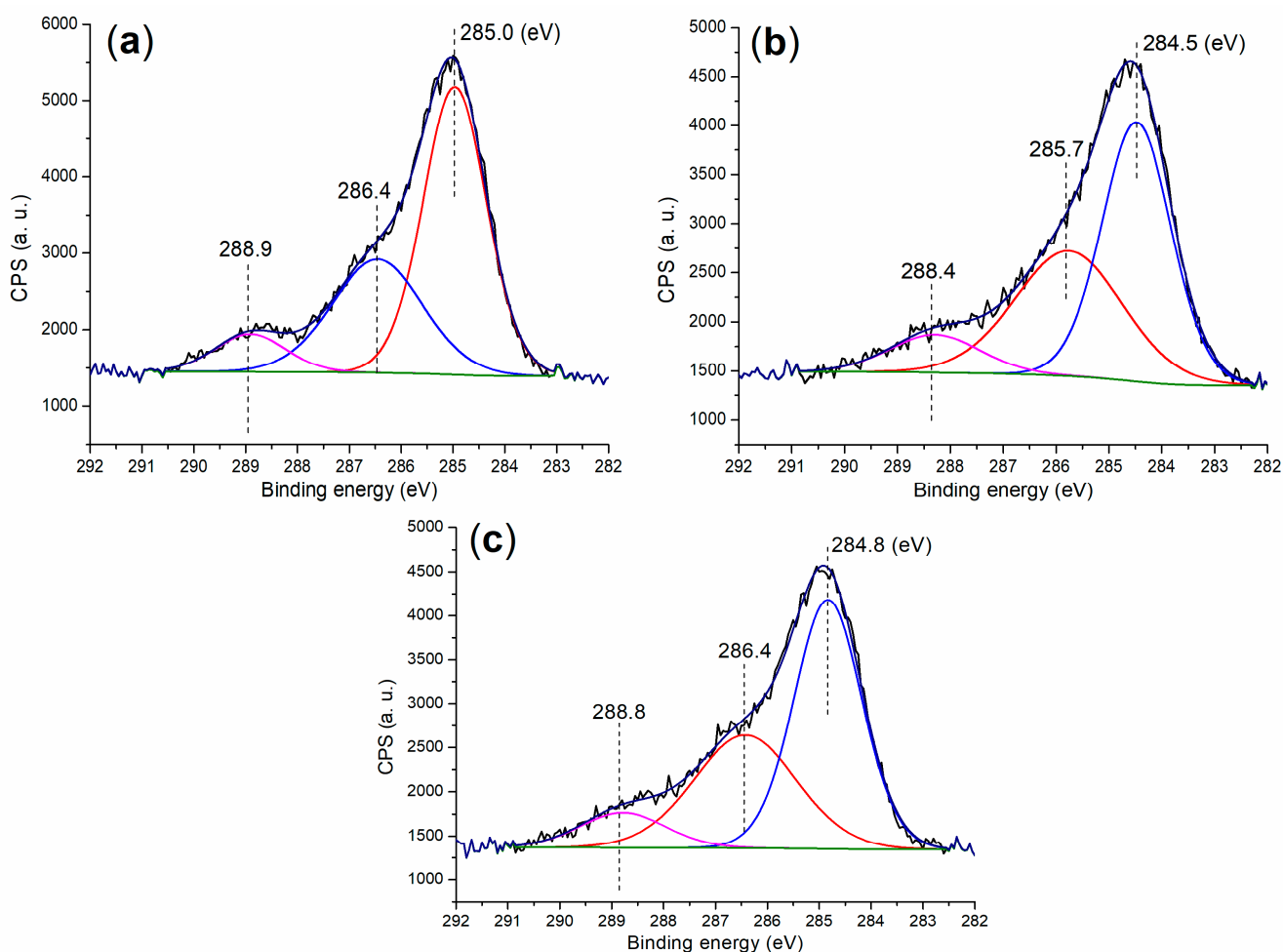


Figure 6. XPS measurement of C 1s region for the synthesized catalysts: (a) C1, (b) C2, (c) C3.

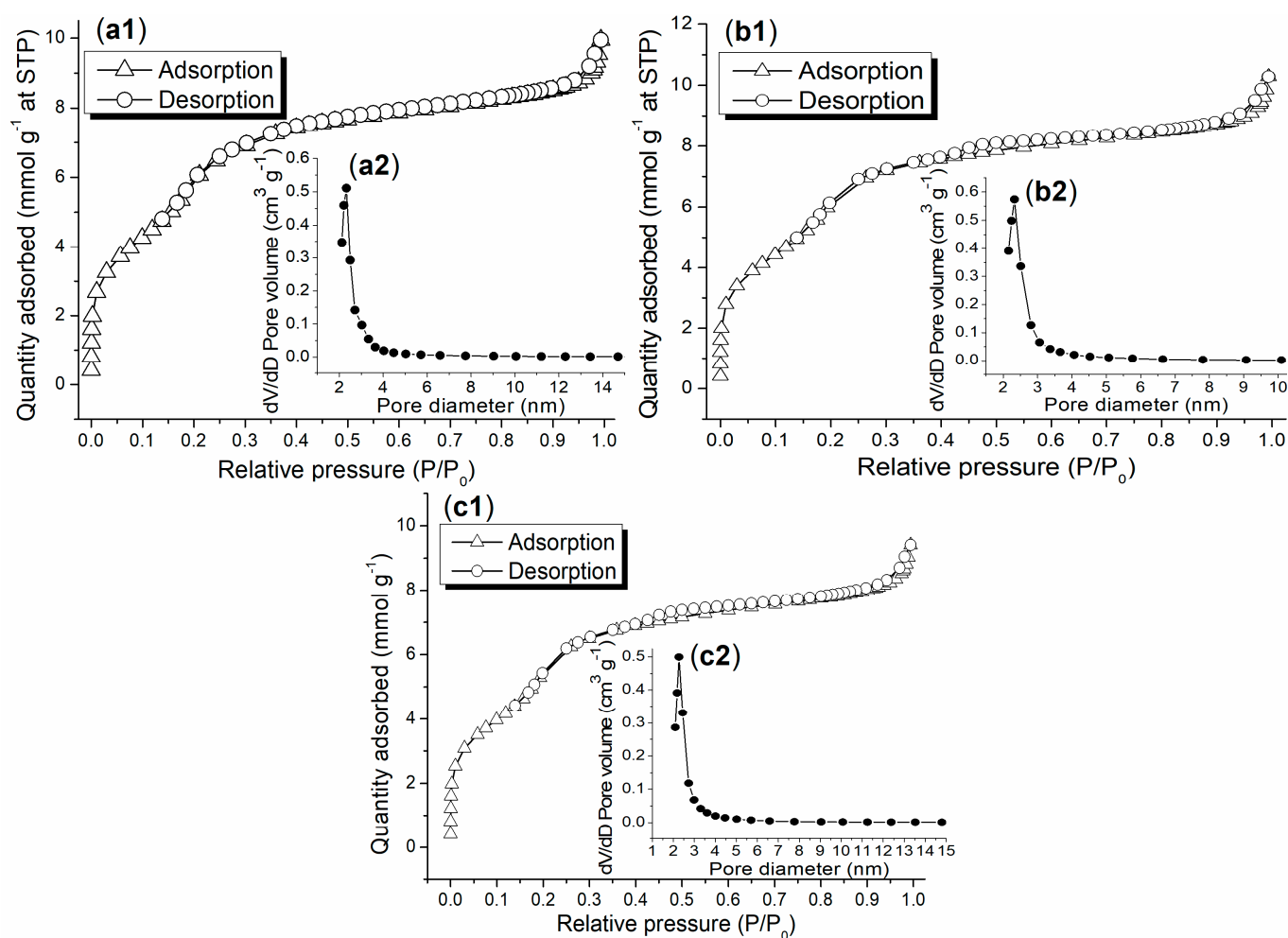


Figure 7. Nitrogen adsorption–desorption isotherms and pore size distributions for synthesized catalysts: (a1,a2) C1, (b1,b2) C2, (c1,c2) C3.

2.4. Functional Group and Thermal Stability of Catalyst

FT-IR spectroscopy provided a powerful tool to detect the functional group of the synthesized catalyst. C1 showed a broad band centered at 3400 cm^{-1} (Figure 8a), characterizing the O-H stretching vibration of the hydroxyl group of (*S*)-binaphthol. The following peak that appeared at 1620 cm^{-1} was indicative of the bending vibration of the hydroxyl group of (*S*)-binaphthol [40]. C1 further showed a series of vibrations at 1050 , 963 , and 797 cm^{-1} (Figure 8a), indicative of Si-O stretching vibrations with different symmetries [41]. Finally, the peak that occurred at 438 cm^{-1} should be assigned to Sn-O vibration (Figure 8a) [25].

The other synthesized catalysts (C2–C3) showed similar FT-IR spectra as C1 (Figure 8b,c vs. Figure 8a), indicating that they contained the same silicate skeletons (Scheme 1). However, catalysts C2–C3 showed stretching vibrations of metal–O bonds at wavenumbers higher than the value of 438 cm^{-1} found for C1 (Figure 8b,c vs. Figure 8a), mainly due to the influences of different synthetic additives or attached ligands in the sol-gel synthesis (Scheme 1).

Thermal analyses, including TGA and DSC, were used to determine the organic species content in the synthesized catalysts, as well as the thermal stability. C1 showed weight loss of 26.71% at $30\text{--}350\text{ }^{\circ}\text{C}$ (black line, Figure 9a), which was propelled by a broad endothermic band that appeared at $50\text{--}150\text{ }^{\circ}\text{C}$ (black line, Figure 9b), indicating the departure of the attached ligand under continuous heating (C1, Scheme 1). The subsequent weight loss of 9.61% at $350\text{--}800\text{ }^{\circ}\text{C}$ (black line, Figure 9a) represented the removal of involatile organic residues derived from the sol-gel synthesis (Scheme 1).

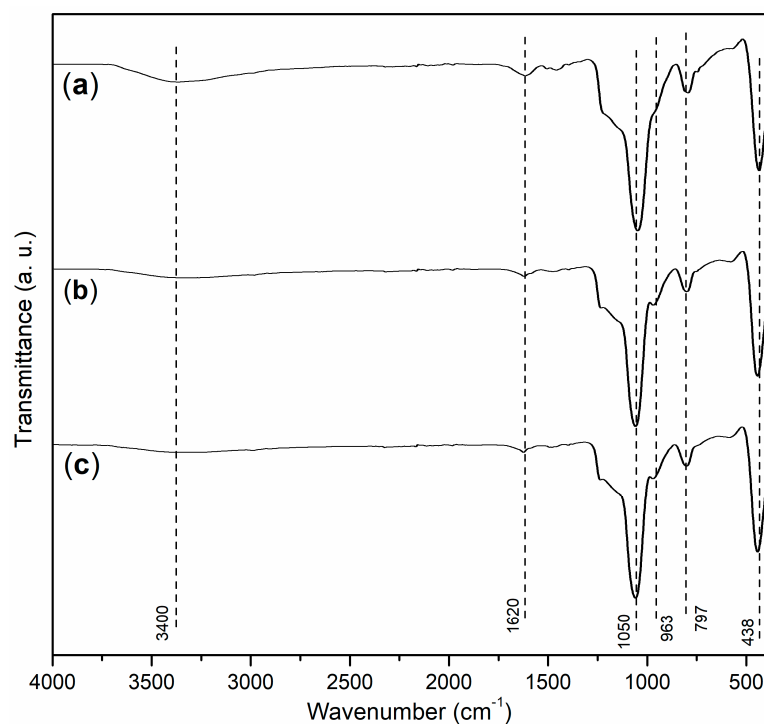


Figure 8. FT-IR spectra of the synthesized catalysts: (a) C1, (b) C2, (c) C3.

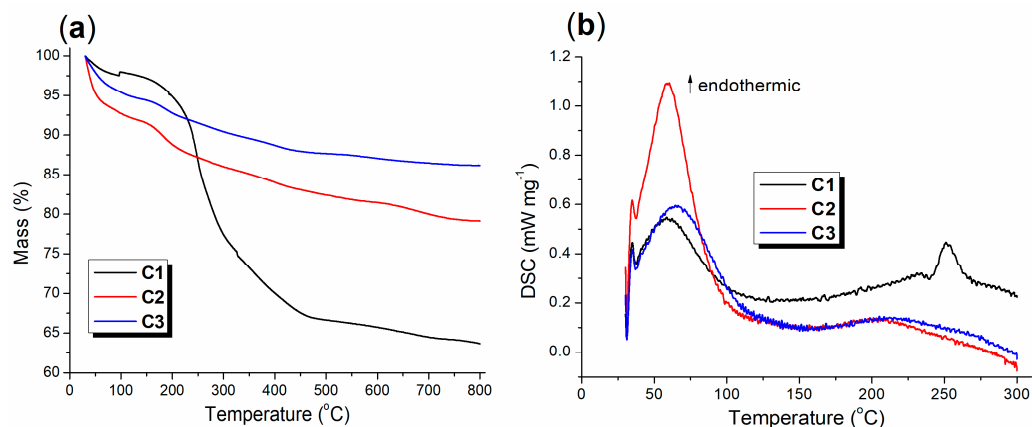


Figure 9. Thermal analysis of the synthesized catalysts: (a) TGA and (b) DSC curves.

The TGA curve of C2 looked quite different from that of C1 because the weight loss in C2 that occurred at 30–800 °C was 20.85%, much lower than that of C1 (red vs. black, Figure 9a), and it was mainly due to the lack of (*L*)-sodium lactate loading in the sol-gel synthesis of C2 (Scheme 1). However, both C1 and C2 showed broad endothermic bands at 50–150 °C (Figure 9b), providing energy for the removal of organic species. Additionally, C3 showed a much slower TGA drop line than C2 in the range of 30–800 °C (blue vs. red, Figure 9a), which clearly proved that C2 contained the attached binaphthol, in contrast to C3 (Scheme 1).

2.5. Morphology and Internal Structure of Catalysts

According to SEM, C1 consisted of particles with sizes of 200–300 nm, along with some aggregates (Figure 10a). TEM further proved that the particles were solid rather than hollow materials (Figure S1a in Section S1 in the Supplementary Materials). C2 had a similar morphology as C1, but the aggregation seemed heavier (Figure 10b vs. Figure 10a), suggesting that the loading of (*L*)-sodium lactate decreased the size of the synthesized

catalyst (C1 vs. C2, Scheme 1). Next, C3 seemed to be more tacky and much larger than C2 (Figure 10c vs. Figure 10b, Figure S1c vs. Figure S1b), and large blocks with sizes of 500 nm to 1 μm occurred (Figure 10c). Thus, the attachment of (*S*)-binaphthol during the sol-gel process promoted the dispersibility of the catalyst particles (C2 vs. C3, Scheme 1).

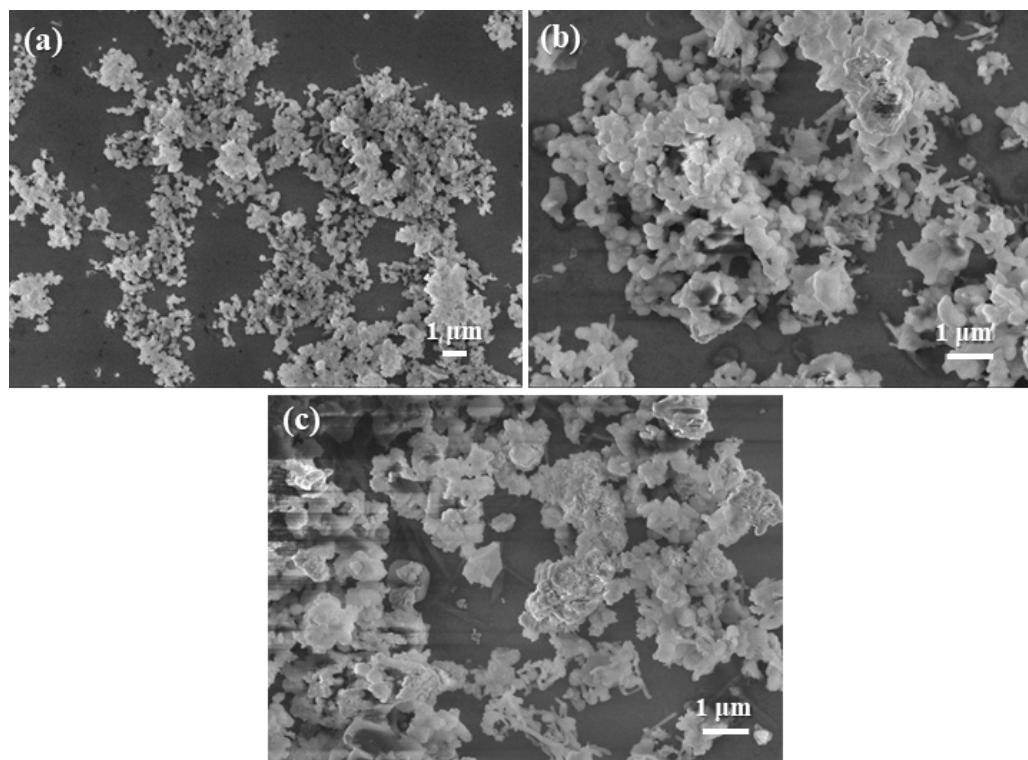


Figure 10. SEM images of synthesized catalysts: (a) C1 (magnification of 5000 \times), (b) C2 (10,000 \times), (c) C3 (10,000 \times).

2.6. Catalytic BVO Reactions

2.6.1. Effect of Substrate

Overall, the structures of the various carbonyl substrates employed in this work played the dominant role in controlling the species and yields of the catalytic products. Firstly, when aliphatic ketones such as CHONE and cyclopentanone were loaded as substrates, the BVO products (lactones) usually appeared to be major products (Tables 4 and 5). Moreover, the ring-opening (hydrolysis) product of lactone (HHA, Table 4) appeared in the BVO of CHONE, probably due to the high tension of the seven-membered lactone ring (ϵ -CL, Table 4) [4]. In comparison, the BVO of cyclopentanone showed no ring-opening product (Table 5 vs. Table 4), probably because the six-membered ring was more stable than the seven-membered one [4].

Secondly, when the substrate was changed from aliphatic ketones to aldehyde (cyclohexanecarbaldehyde), both BVO and aerobic oxidation products occurred (Table 6), indicating that the cyclohexyl group (aliphatic) could stabilize the Criegee intermediate (Figure 1) to some extent under the catalytic conditions employed [6]. However, the catalytic oxidation of benzaldehyde only yielded benzoic acid (Table 7), and no BVO-type oxidation products were found, probably because the phenyl group (aromatic) showed poor Criegee rearrangement activity in the transition state (Figure 1) under the catalytic conditions employed [6].

Table 4. Catalytic BVO of cyclohexanone over synthesized catalysts.

1) Oxidant (2 mmol)
2) Solvent (10 mL)
3) Catalyst (2 mol% metal)
4) 80 °C or 40 °C, 3 h

CHONE → ϵ -CL + HHA

Entry ^a	Oxidant	Solvent	Temperature (°C)	Catalyst	Conversion (%) ^b	Yield (%) ^c	TOF (h ⁻¹) ^d
1	(NH ₄) ₂ S ₂ O ₈	Toluene	80	C2	0	0	0
2		CH ₃ CN	80	C2	23	23 (ϵ -CL)	3.83
3		CH ₃ CN	80	C3	57	14 (ϵ -CL), 43 (HHA)	2.33
4		CH ₂ Cl ₂	40	C2	0	0	0
5		H ₂ O	80	C1	0	0	0
6	<i>m</i> -CPBA	Toluene	80	C1	71	71 (ϵ -CL)	11.83
7		H ₂ O	80	C1	76	76 (ϵ -CL)	12.66
8		H ₂ O	80	C2	88	3 (ϵ -CL), 85 (HHA)	0.50
9		H ₂ O	80	C3	100	100 (ϵ -CL)	16.66
10	H ₂ O ₂ (30%)	CH ₂ Cl ₂	40	C1	0	0	0

^a Experimental details as shown in Section 3.4; cyclohexanone (CHONE), 2 mmol. ^b Conversion of CHONE to all possible products, as determined by GC-MS (Figures S2 and S3 in Section S2 in the Supplementary Materials). ^c Yield of each product based on the substrate, as determined by GC-MS (Section S2 in the Supplementary Materials). ^d Turnover frequency for ϵ -CL, mol _{ϵ -CL} mol_{Sn of catalyst}⁻¹ (time, h)⁻¹.

Table 5. Catalytic BVO of cyclopentanone over synthesized catalysts.

1) Oxidant (2 mmol)
2) CH₃CN (10 mL)
3) Catalyst (2 mol% metal)
4) 80 °C or 40 °C, 3 h

Cyclopentanone → ϵ -CL

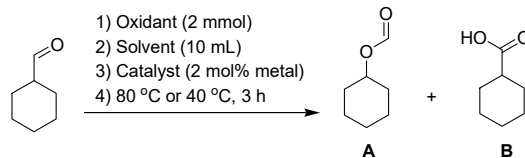
Entry ^a	Oxidant	Temperature (°C)	Catalyst	Conversion (%) ^b	Yield (%) ^c	TOF (h ⁻¹) ^d
1	<i>m</i> -CPBA	40	None	6	6	1.00
2		80	None	14	14	2.33
3		80	C1	42	42	7.00
4		80	C2	100	100	16.66
5		40	C2	30	30	5.00
6		80	C3	100	100	16.66
7		40	C3	87	87	14.50
8	H ₂ O ₂ (30%)	80	C1	12	12	2.00
9		80	None	0	0	0

^a Experimental details as shown in Section 3.4; cyclopentanone, 2 mmol. ^b Conversion of cyclopentanone (substrate) to all possible products, as determined by GC-MS (Figures S4 and S5 in Section S3 in the Supplementary Materials). ^c Yield of each product based on the substrate, as determined by GC-MS (Section S3 in the Supplementary Materials). ^d Turnover frequency for BVO product, mol_{BVO product} mol_{Sn of catalyst}⁻¹ (time, h)⁻¹.

2.6.2. Effect of the Oxidant

The oxidant also showed important influences on the outputs under the catalytic BVO conditions employed. At first, when CHONE was employed as the substrate, regardless of the solvent, the oxidants preferred BVO-type conversion in the order *m*-CPBA > (NH₄)₂S₂O₈ > H₂O₂ (30%) (Table 4). Moreover, this order remained almost the same for the transformation of cyclopentanone (Table 5). When the substrate was changed to cyclohexanecarbaldehyde, the comparison of oxidants still indicated the same tendency (Table 6). This order was also confirmed for the pure aerobic oxidation of benzaldehyde (Table 7).

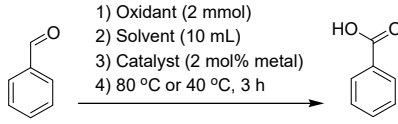
Table 6. Catalytic Baeyer–Villiger oxidation and aerobic oxidation of cyclohexanecarbaldehyde over synthesized catalysts.



Entry ^a	Oxidant	Solvent	Temperature (°C)	Catalyst	Conversion (%) ^b	Yield (%) ^c
1	(NH ₄) ₂ S ₂ O ₈	Toluene	80	C1	65	7 (A), 58 (B)
2		Toluene	80	C2	33	6 (A), 27 (B)
3		CH ₂ Cl ₂	40	C1	60	10 (A), 50 (B)
4		CH ₂ Cl ₂	40	C2	66	11 (A), 55 (B)
5		H ₂ O	80	C1	98	98 (B)
6	<i>m</i> -CPBA	CH ₃ CN	80	C2	66	19 (A), 47 (B)
7		CH ₃ CN	80	C3	81	14 (A), 67 (B)
8		CH ₂ Cl ₂	40	C1	78	41 (A), 37 (B)
9		H ₂ O	80	C2	94	94 (B)
10		H ₂ O	80	C3	83	83 (B)
11	H ₂ O ₂ (30%)	CH ₂ Cl ₂	40	C1	60	2 (A), 58 (B)
12		CH ₂ Cl ₂	40	C3	57	11 (A), 46 (B)

^a Experimental details as shown in Section 3.4; cyclohexanecarbaldehyde, 2 mmol. ^b Conversion of cyclohexanecarbaldehyde (substrate) to all possible products, as determined by GC-MS (Figures S6–S10 in Section S4 in the Supplementary Materials). ^c Yield of each product based on the substrate, as determined by GC-MS (Section S4 in the Supplementary Materials).

Table 7. Catalytic aerobic oxidation of benzaldehyde over synthesized catalysts.



Entry ^a	Oxidant	Solvent	Temperature (°C)	Catalyst	Conversion (%) ^b	Yield (%) ^c
1	(NH ₄) ₂ S ₂ O ₈	Toluene	80	C3	50	50
2		CH ₂ Cl ₂	40	C2	68	68
3		CH ₃ CN	80	C2	79	79
4	<i>m</i> -CPBA	Toluene	80	C1	88	88
5		Toluene	80	C2	54	54
6		H ₂ O	80	C1	45	45
7		CH ₂ Cl ₂	40	C1	56	56
8		CH ₂ Cl ₂	40	C2	22	22
9	H ₂ O ₂ (30%)	CH ₂ Cl ₂	40	C1	52	52

^a Experimental details as shown in Section 3.4; benzaldehyde, 2 mmol. ^b Conversion of benzaldehyde (substrate) to all possible products, as determined by GC-MS (Figure S11 in Section S5 in the Supplementary Materials). ^c Yield of each product based on the substrate, as determined by GC-MS (Section S5 in the Supplementary Materials).

It has previously been reported that the peracid-like *m*-CPBA is the most widely applied oxidant for BVO [1]. When CHONE was used as the substrate in this work, the effects of *m*-CPBA on the BVO were comparable to or higher than those reported previously (entries 6–7, Table 4) [1,4]. Furthermore, very high BVO conversions were obtained with *m*-CPBA as the oxidant in the transformation of cyclopentanone (entries 4 and 6, Table 5), much higher than previously reported results [1,4]. Obviously, *m*-CPBA had great synergy with the present synthesized catalysts for the BVO of aliphatic ketones.

The (NH₄)₂S₂O₈ used in this work showed moderate to high conversions of BVO and aerobic oxidation (Tables 4, 6 and 7), highly comparable to those obtained when using peroxomonosulfate (KHSO₅) as the terminal oxidant [24]. Moreover, no by-products were

found in $(\text{NH}_4)_2\text{S}_2\text{O}_8$ -facilitated reactions (Tables 4, 6 and 7), contributing to the final product purification.

2.6.3. Effect of the Solvent

Following the analysis of the reaction parameters presented so far, it is also necessary to discuss the effect of the solvent to achieve optimization. No matter which catalyst was used, when CHONE was used as the substrate with *m*-CPBA as the oxidant, both toluene and H_2O seemed to be available for the BVO (entries 6–9, Table 4). With $(\text{NH}_4)_2\text{S}_2\text{O}_8$, CH_3CN was most effective, but other solvents, including toluene, CH_2Cl_2 , and H_2O , were unsuitable (entries 1, 4, and 5, Table 4). Furthermore, CH_2Cl_2 was also invalid for the H_2O_2 -oxidized conversion (entry 10, Table 4). When cyclopentanone was selected as the substrate, CH_3CN worked well in combination with both *m*-CPBA and H_2O_2 (entries 1–8, Table 5). On the basis of the above results, it can be seen that the miscibility of the solvent with the oxidant affected the BVO efficiency of the aliphatic ketones. Obviously, the better the miscibility was, the higher the BVO outputs obtained.

For the transformation of aliphatic aldehyde (cyclohexanecarbaldehyde), using H_2O as a solvent only gave an aerobic oxidation product, regardless of the oxidant (entries 5, 9, and 10, Table 6), while organic solvents, such as toluene, CH_2Cl_2 , and CH_3CN , could give BVO-type products (entries 1–4, 6–8, and 11–12, Table 6). Thus, it seemed that aerobic oxidation preferred an aqueous environment to an organic solvent, and the Criegee intermediate originating from an aliphatic aldehyde substrate may be better stabilized in organic solvent than in H_2O [6].

When aromatic aldehyde (benzaldehyde) was introduced as a substrate, no BVO-type transformations appeared with any of the parameter settings, including the oxidant, solvent, catalyst, and temperature (Table 7), clearly indicating that the Criegee intermediate derived from benzaldehyde could not be well-established with the catalytic system employed (Figure 1) [6]. Instead, moderate to high aerobic oxidation yields were obtained (Table 7). When $(\text{NH}_4)_2\text{S}_2\text{O}_8$ was employed as the terminal oxidant, the solvent order was $\text{CH}_3\text{CN} > \text{CH}_2\text{Cl}_2 > \text{toluene}$ (entries 1–3, Table 7), which changed to $\text{toluene} > \text{CH}_2\text{Cl}_2 > \text{H}_2\text{O}$ with *m*-CPBA as the oxidant (entries 4–8, Table 7). Obviously, the miscibility of the solvent with the oxidant affected the outputs of the aerobic oxidation of benzaldehyde.

2.6.4. Effects of Temperature and Catalyst

In addition to the substrate, oxidant, and solvent, both the temperature and catalyst showed important influences on catalytic oxidation. First of all, when cyclopentanone was selected as the substrate with *m*-CPBA as the oxidant and CH_3CN as the solvent, the catalyst-blank reaction carried out at $80\text{ }^\circ\text{C}$ seemed to be better than that at $40\text{ }^\circ\text{C}$ (entries 2 vs. 1, Table 5). Furthermore, even in the presence of a catalyst, a higher temperature still resulted in better BVO conversion than a lower one (entries 4 vs. 5 and 6 vs. 7, Table 5). Therefore, it seemed that the higher reaction temperature contributed to the formation of the Criegee intermediate by activating *m*-CPBA [6].

For the comparison of the catalysts, when the temperature was fixed at $80\text{ }^\circ\text{C}$, the reactions featuring C1, C2, and C3 as the catalyst showed much higher BVO conversions than the catalyst-blank reaction (entries 3, 4, and 6 vs. 2, Table 5), clearly indicating that the Lewis acid centers (Sn) on the surface of the synthesized catalysts were coordinated by cyclopentanone, the carbonyl group of which was activated subsequently, as has been revealed by Corma and co-workers [17]. Moreover, hydrogen peroxide (H_2O_2 , 30%) could not oxidize cyclopentanone alone (entries 9 vs. 8, Table 5), further proving that the coordination and activation of the carbonyl group over the Sn center of the catalyst played a key role in the BVO-type transformation.

On the other hand, C2 showed much better BVO conversion than C1 in the transformation of cyclopentanone (entries 4 vs. 3, Table 5). Similarly, better BVO conversion of CHONE was obtained when using C2 than C1 with *m*-CPBA as the oxidant in water at $80\text{ }^\circ\text{C}$ (entries

8 vs. 7, Table 4). Both of these findings can be ascribed to the higher BET surface area, pore volume, and pore radius of C2 compared to C1 (C2 vs. C1, Table 2), reflecting the negative effects of the loading of (*L*)-sodium lactate on the porosity of the sol-gel product (C1 vs. C2, Scheme 1).

Furthermore, C3 performed much better than C2 in the BVO conversion of cyclopentanone with *m*-CPBA as the oxidant at 40 °C (entries 7 vs. 5, Table 5). Moreover, when CHONE was oxidized in CH₃CN at 80 °C with (NH₄)₂S₂O₈ as the terminal oxidant, C3 showed better BVO conversion than C2 (entries 3 vs. 2, Table 4). The same trend was also found in the same transformation with *m*-CPBA as the oxidant in water at 80 °C (entries 9 vs. 8, Table 4). Thus, it can be seen that the attachment of binaphthol to the Sn-containing silicate backbone reduced the BVO outputs of aliphatic ketones (C3 vs. C2, Scheme 1), probably because the coordinated binaphthol occupied the empty orbitals of Sn on the catalyst surface, which inhibited the activation of the ketone substrate.

However, when aliphatic aldehyde (cyclohexanecarbaldehyde) was employed as the substrate, C1 performed better than C2 with (NH₄)₂S₂O₈ as the oxidant in toluene (entries 1 vs. 2, Table 6), and their activities became close in CH₂Cl₂ (entries 3 vs. 4, Table 6). At the same time, C2 showed better BVO conversion (product A as standard, Table 6) than C3 with *m*-CPBA as the oxidant in CH₃CN (entries 6 vs. 7, Table 6), and C2 still seemed better than C3 for pure aerobic oxidation in H₂O (entries 9 vs. 10, Table 6). On the other hand, for the aerobic oxidation of aromatic aldehyde (benzaldehyde) using *m*-CPBA as the oxidant, C1 performed better than C2 in both toluene (entries 4 vs. 5, Table 7) and CH₂Cl₂ (entries 7 vs. 8, Table 7).

In view of these results, along with the sol-gel synthesis conditions for C1–C3 (Scheme 1), it seems reasonable that the Criegee intermediate of aliphatic aldehyde could be stabilized by the attached binaphthol of the catalyst in the transition state, finally leading to better BVO efficiency, which also contributed to the aerobic oxidation of the carbonyls of aliphatic and aromatic aldehydes.

From another point of view, when CHONE was used as a substrate with H₂O₂ as the terminal oxidant, catalyst C1 was completely inert (entry 10, Table 4), which was not comparable to the moderate BVO-type yields and TOF values achieved with hierarchical FAU-type stannosilicate [23] and rapidly synthesized Sn-beta zeolites [20]. When the substrate was changed to cyclopentanone with the same terminal oxidant, the BVO-type yield and TOF values obtained with C1 were a little lower than those from a phosphorous-doped graphitic catalyst [42]. However, when *m*-CPBA was used as the terminal oxidant instead of H₂O₂, the catalytic BVO-type conversions of CHONE and cyclopentanone were improved significantly (entries 6–9 vs. 10, Table 4; entries 1–7 vs. 8–9, Table 5).

On the other hand, although high values for HHA have been confirmed in many fields, there are very few reports on the effective direct oxidation of CHONE into HHA [26]. For example, TS-1 has been widely used as a heterogeneous catalyst for oxidation of CHONE, but only a mixture of ϵ -CL, HHA, and AA and low total conversion were obtained [29]. However, the catalysts C3 and C2 synthesized here showed moderate to high yields of HHA with inorganic ((NH₄)₂S₂O₈, entry 3, Table 4) and organic (*m*-CPBA, entry 8, Table 4) terminal oxidants, respectively, which is significant for future large-scale applications.

Additionally, cyclohexylformate appears to be a key intermediate for the production of high-value-added cyclohexanol [33], and the known preparation of cyclohexylformate was derived from the addition of formic acid to cyclohexene [33]. To the best of our knowledge, there are no reports on the direct transformation of cyclohexanecarbaldehyde to cyclohexylformate through BVO, probably because the dominant product appears to be cyclohexanecarboxylic acid (product B, Table 6) [33]. However, C1 could catalyze the BVO of cyclohexanecarbaldehyde to cyclohexylformate with *m*-CPBA as the terminal oxidant in CH₂Cl₂, yielding 78% total substrate conversion and cyclohexylformate as the dominant product (entry 8, Table 6).

2.7. Possible Reaction Pathway for Catalytic BVO of Cyclohexanone

In order to further elucidate the formation of 6-hydroxyhexanoic acid with the SnO₂ nanoparticles of the synthesized catalyst (HHA, entry 8, Table 4), a possible reaction process is proposed in Figure 11. First of all, the Sn-beta zeolite framework can be considered as a reference when simulating a catalyst surface [43], for which the hydroxyl open site has previously been confirmed to be more active than the closed site (catalyst, Figure 11) [44]. Next, on the basis of the effects of the catalysts revealed previously (for example, entries 2–3 and 7–9, Table 4), it can be seen that the Sn centers fixed on the catalyst surface play a key role in activating oxidants such as *m*-CPBA, for which the silanol group on the catalyst was oxidized to the peroxy group (A, Figure 11).

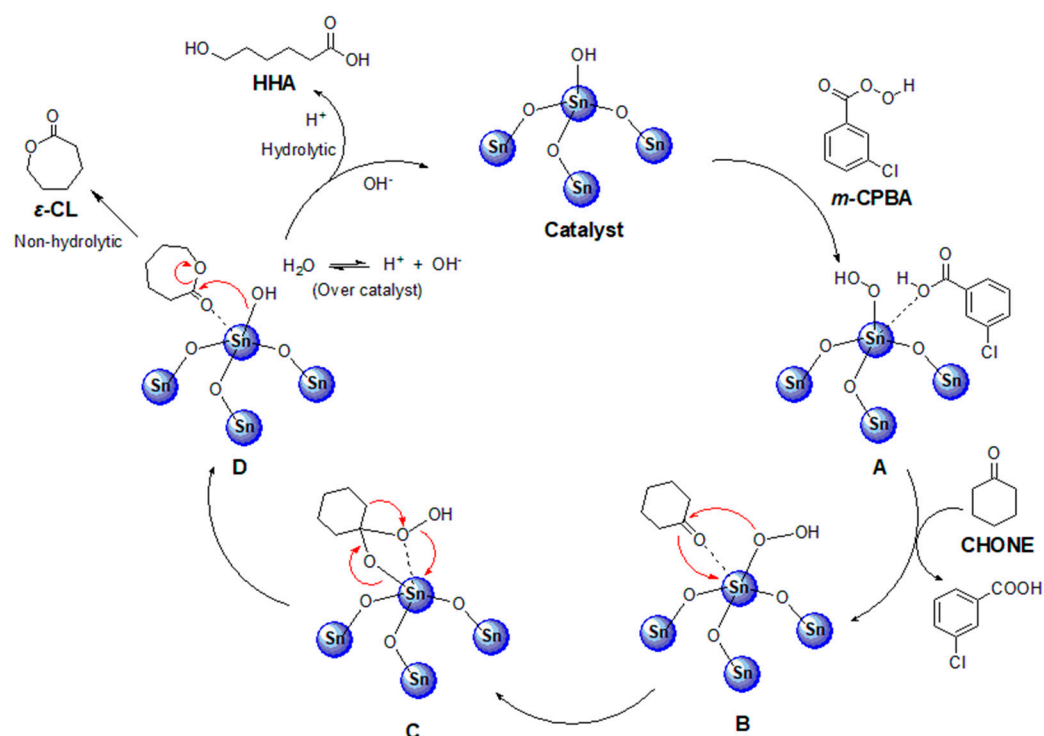


Figure 11. The favored reaction process for the BVO-type transformation of cyclohexanone (CHONE) with *m*-CPBA as the oxidant catalyzed by SnO₂ nanoparticles.

After the introduction of cyclohexanone, the coordinating linkage of the carbonyl group with the Sn center provided a platform for rearrangement that led to ϵ -CL, the lactone product (B–D, Figure 11). However, simultaneously, the recovered silanol group attacked the carbon of the carbonyl group of ϵ -CL again and, subsequently, 6-hydroxyhexanoic acid (HHA) was formed in association with the acidic medium (D, Figure 11). In this process, water coming from either the solvent or the atmosphere may be ionized over the Sn center of the catalyst, eventually contributing to the recovery of the active Sn-containing catalyst (D to catalyst, Figure 11).

3. Experimental Section

3.1. Starting Materials

The tin(II) chloride (SnCl₂, anhydrous, 99%) was purchased from Acros (Acros Organics, part of Thermo Fisher Scientific, Thermo Fisher Scientific (China) Co., Ltd., Shanghai, China). The cetyltrimethylammonium bromide (CTAB, 99%), (*L*)-sodium lactate (99%), and tetraethyl orthosilicate (TEOS, 99%) were commercially available from Alfa Aesar (part of Thermo Fisher Scientific, Thermo Fisher Scientific (China) Co., Ltd., Shanghai, China). The (*S*)-(-)-binaphthol (98%), cyclohexanone (CHONE, 99%), cyclopentanone (99%), cyclohexanecarboxaldehyde (97%), and benzaldehyde (99%) were bought from Sigma-Aldrich

(Sigma Aldrich (Shanghai) Trading Co., Ltd., Shanghai, China). The *m*-chloroperoxybenzoic acid (*m*-CPBA, 75%), ammonium persulfate ((NH₄)₂S₂O₈, 98%), hydrogen peroxide (H₂O₂, 30 wt.% solution in water), and ammonium hydroxide solution (NH₃·H₂O, 25 wt.% solution in water) were purchased from Fluka (Honeywell International Inc., Seelze, Germany). Other solvents were supplied by local suppliers and purified before use in our laboratories.

3.2. Instruments and Analytical Methods

X-ray photoelectron spectroscopy (XPS) was used to determine the elemental composition and chemical state on the surface of the solid catalyst (depth of 0–3 nm). It was carried out on a Kratos Axis Ultra DLD (Kratos Co., Ltd., Manchester, UK) using monochromatic Al K α X-rays (1486.6 eV) as the lighting source, and the binding energy scale was calibrated by setting the C 1s peak at 284.8 eV. Furthermore, the peaks were fitted by using the Gaussian–Lorentz (G/L) product function with a 30% Lorentzian ratio. Wide-angle ($2\theta = 10$ – 80°) X-ray diffractions were employed to obtain crystallinity information for the solid catalyst using a Philips X'Pert Pro diffractometer (PANalytical B.V. Co., Ltd., Almelo, Holland) with Cu-K α radiation ($\lambda = 1.5418 \text{ \AA}$) and an interval of $0.05^\circ \text{ s}^{-1}$.

The BET surface area, pore volume, pore diameter, and pore size distribution provided key information on the catalysts' porosity and internal structure and were measured with a Micromeritics ASAP 2020 (Micromeritics Instruments Corporation, Norcross, Atlanta, GA, USA) on the basis of the N₂ adsorption isotherms at 77.35 K. Synthesized catalysts were degassed at 150 °C in a vacuum before testing. Surface area was calculated by applying the multi-point Brunauer–Emmett–Teller (BET) method to the adsorption data with relative pressure P/P_0 of 0.06–0.3. Total pore volume was obtained from N₂ that adsorbed at $P/P_0 = 0.97$. Both the pore volume and pore diameter were obtained by employing the Barrett–Joyner–Halenda (BJH) method.

The size and zeta potential of the solvated catalyst particles indicated the catalysts' stability in solvent and were measured on a Malvern Zetasizer Nano ZS90 spectrometer (Malvern, UK). The amounts of acid (both Lewis and Brønsted acidity) in the synthesized catalysts were determined following a reported method with some modifications [45] by employing *n*-butylamine titration with coeruleum bromocresolis as the indicator, and the method can determine the catalyst activity to some extent. In practice, the solid catalyst (300 mg) was first combined with *n*-butylamine (0.05 mol L^{−1} solution in toluene, 25.00 mL) in a conical flask (250 mL). After shaking for 5 min under a cover, 2-propanol (100 mL) and coeruleum bromocresolis (one drop, diluted solution) were added together. The resulting solution was then titrated with HCl solution (0.025 mol L^{−1} in water), and the end point of the titration was determined when the solution color changed from blue to yellow. The amount of acid in the sample was viewed as the amount of *n*-butylamine adsorbed and was calculated by subtraction of the residues in the solution determined by HCl titration from the total *n*-butylamine.

The FT-IR method is a powerful tool for detecting the organic functional groups of synthesized catalysts, and it was employed when the sample was dispersed into KBr pellets on a Bruker Tensor 27 (BRUKER equipment, Bremen, Germany) with wavenumbers of 400–4000 cm^{−1}. Thermogravimetric analysis (TGA) was undertaken on a NETZSH TG 209C (NETZSH Corporation, Bavaria, Germany) with a TASC 414/4 controller under N₂ protection, using a heating rate of 10 °C min^{−1} in the range of 30–800 °C. Differential scanning calorimetry (DSC) was undertaken on a NETZSH DSC 214 (NETZSH Corporation, Bavaria, Germany) with N₂ protection, using a heating rate of 10 °C min^{−1} in the range of 30–300 °C. These two thermal analyses not only showed the catalyst stability during heating but also presented the chemical composition from another point of view. The scanning electron microscopy (SEM) was undertaken on a JEOL JSM-6700F (JEOL Ltd., Tokyo, Japan) at 20.0 kV in the absence of a Au coating. Transmission electron microscopy (TEM) was undertaken on a JEOL JEM-200CX (JEOL Ltd., Tokyo, Japan) at 120 kV.

The BVO conversions and product yields in this work were determined with a GCMS-QP2010 Plus (Shimadzu) using an Rxi-5ms capillary column with a length of 30 m and

internal diameter of 0.25 mm. For the GC, the column temperature was set to 60 °C, the injection port temperature was adjusted to 250 °C, the sampling mode was split-flow, the split ratio was 26, and He was employed as the carrier gas. For the MS, the ion source temperature was 200 °C and the interface temperature was set to 250 °C.

3.3. Synthesis of Sn-Containing Silicate Catalysts

As shown in Scheme 1, the anhydrous SnCl₂ (C1–C3, 0.5 mmol), cetyltrimethylammonium bromide (CTAB, 0.4 g, 1.09 mmol), and (*L*)-sodium lactate (C1, 0.43 mmol; C2–C3, 0 mmol) were combined with NH₃·H₂O (25 wt.% solution in water, 100 mL) in a round-bottomed flask (250 mL). After stirring at 25 °C for 1 h, tetraethyl orthosilicate (TEOS, 2 mL, 1.88 g, 9.02 mmol) was introduced, and the resulting sol was continuously stirred at 40 °C for 3 h. Subsequently, the whole sol was transferred into an autoclave (125 mL) and then aged at 100 °C for 24 h. After being cooled to room temperature, the solids were collected by filtration under reduced pressure and washed with distilled water (3 × 20 mL) and absolute ethanol (3 × 20 mL). The washed solids were finally calcined at 550 °C for 5 h in a muffle oven and then collected for further modification.

Next, the calcined solid (0.5 g), triethylamine (2.02 g, 20 mmol), and (*S*)-binaphthol (C1–C2, 2.49 mmol; C3, 0 mmol) were mixed with dry toluene (100 mL) in a round-bottomed flask (250 mL). The mixture was refluxed at 80 °C for 9 h. After being cooled to room temperature, the solids were collected by filtration under reduced pressure, washed with distilled water (3 × 20 mL) and absolute ethanol (3 × 20 mL), and then dried at 90 °C for 6 h in a baking oven, finally yielding C1 (0.61 g), C2 (0.55 g), and C3 (0.53 g), respectively.

3.4. Catalytic BVO Reaction

The carbonyl substrate (2.0 mmol, including cyclohexanone, cyclopentanone, cyclohexanecarboxaldehyde, and benzaldehyde) was mixed with solvent (10 mL, including toluene, CH₃CN, CH₂Cl₂, and H₂O) in a round-bottomed flask (100 mL) under magnetic stirring at room temperature. The oxidant (2.0 mmol of (NH₄)₂S₂O₈, *m*-CPBA, or H₂O₂) and catalyst (2 mol% Sn over a substrate for C1–C3; based on XPS data from Table 1) were added together. The mixture obtained was further stirred at a pre-set temperature (80 °C or 40 °C) for 3 h. When the time was up, the mixture was filtrated under reduced pressure, and the filtrate was detected using GC-MS for both identification and quantification.

4. Conclusions

A series of Sn-containing silicate catalysts were prepared using cetyltrimethylammonium bromide as the structure-directing agent, (*L*)-sodium lactate as the crystallization reagent, and anhydrous tin(II) chloride as the Sn precursor through a sol-gel process. The post-synthetic modification of the synthesized catalyst was realized through the coordinated attachment of (*S*)-binaphthol. Comprehensive characterizations revealed that loading of (*L*)-sodium lactate in the sol-gel synthesis not only improved the incorporation efficiency of Sn but also decreased the crystal size of the synthesized catalyst. There were SnO₂ nanoparticles with sizes ranging between 17 and 19 nm on the synthesized catalysts, and the synthesized catalysts had silt-like mesoporous structures. Furthermore, O-containing ligands, such as (*S*)-binaphthol, were attached to the Sn on the catalyst surface.

In the catalysis, when aliphatic ketones such as cyclohexanone and cyclopentanone were used as the substrate, BVO-type products and derivatives were obtained. However, BVO of aliphatic aldehyde (cyclohexanecarbaldehyde) produced both an aerobic oxidation product (carboxylic acid) and BVO-type product. Furthermore, the reported transformation of aromatic aldehyde (benzaldehyde) only gave an aerobic oxidation product (benzoic acid). Furthermore, the miscibility of the solvent with the oxidant affected the BVO efficiency of the aliphatic ketones; the better their miscibility was, the higher the BVO outputs obtained. On the other hand, the post-synthetic coordinating attachment of (*S*)-binaphthol to the Sn-containing silicate backbone worsened the BVO of aliphatic ketones but improved the BVO of aliphatic aldehyde and the aerobic oxidation of aromatic aldehyde. Finally, a

possible reaction pathway for the catalytic BVO of cyclohexanone was proposed to explain the formation of ϵ -CL and HHA under the reported catalytic conditions, and the hydroxyl in the open site of the catalyst surface may have played a key role in activating *m*-CPBA and facilitating BVO transformation.

In addition to the aforementioned results, this work also highlighted two new routes for the catalytic synthesis of 6-hydroxyhexanoic acid and cyclohexylformate under BVO conditions. In sum, this work prepared an interesting series of Sn-containing silicate catalysts to improve the catalytic BVO of versatile carbonyl compounds, and new methods were found for the synthesis of valuable molecules, showing great potential for future large-scale applications.

Supplementary Materials: The following supporting information can be downloaded at: <https://www.mdpi.com/article/10.3390/catal13050805/s1>, Figure S1: TEM images of synthesized catalysts: (a) C1 (magnification of 27,000 \times), (b) C2 (27,000 \times), (c) C3 (80,000 \times); Figure S2: GC part of GC-MS for Entry 2, Table 4; Figure S3: GC part of GC-MS for Entry 3, Table 4; Figure S4: GC part of GC-MS for Entry 1, Table 5; Figure S5: GC part of GC-MS for Entry 7, Table 5; Figure S6: GC part of GC-MS for Entry 2, Table 6; Figure S7: GC part of GC-MS for Entry 3, Table 6; Figure S8: GC part of GC-MS for Entry 4, Table 6; Figure S9: GC part of GC-MS for Entry 8, Table 6; Figure S10: GC part of GC-MS for Entry 12, Table 6; Figure S11: GC part of GC-MS for Entry 2, Table 7.

Author Contributions: Experimental and sample analysis, J.M.; experimental and sample analysis, A.Z.; experiment design and methodology, Q.P.; material characterization, Y.W.; sample analysis and funding acquisition, X.W.; experiment design and methodology, X.L.; catalytic reaction, W.W.; material characterization, M.G.; conceptualization and original draft preparation, Y.S. All authors have read and agreed to the published version of the manuscript.

Funding: This study was supported by the Natural Science Basic Research Program of Shaanxi Province (No. 2020JM-019).

Data Availability Statement: The data presented in this study are available on request from the corresponding author.

Conflicts of Interest: The authors declare no conflict of interest.

References

1. Renz, M.; Meunier, B. 100 Years of Baeyer-Villiger oxidations. *Eur. J. Org. Chem.* **1999**, *1999*, 737–750. [[CrossRef](#)]
2. Wang, B.; Shen, Y.-M.; Shi, Y. Enantioselective synthesis of γ -aryl- γ -butyrolactones by sequential asymmetric epoxidation, ring expansion, and Baeyer-Villiger oxidation. *J. Org. Chem.* **2006**, *71*, 9519–9521. [[CrossRef](#)]
3. Winkler, M.; Raupp, Y.S.; Köhl, L.A.M.; Wagner, H.E.; Meier, M.A.R. Modified poly(ϵ -caprolactone)s: An efficient and renewable access via thia-michael addition and Baeyer–Villiger oxidation. *Macromolecules* **2014**, *47*, 2842–2846. [[CrossRef](#)]
4. ten Brink, G.-J.; Arends, I.W.C.E.; Shelton, R.A. The Baeyer-Villiger reaction: New developments toward greener procedures. *Chem. Rev.* **2004**, *104*, 4105–4124. [[CrossRef](#)] [[PubMed](#)]
5. Fries, S.L.; Farnham, N. Reactions of peracids. IV. The reaction of cyclohexylphenyl ketone with perbenzoic acid. *J. Am. Chem. Soc.* **1950**, *72*, 5518–5521. [[CrossRef](#)]
6. Grein, F.; Chen, A.C.; Edwards, D.; Crudden, C.M. Theoretical and experimental studies on the Baeyer-Villiger oxidation of ketones and the effect of γ -halo substituents. *J. Org. Chem.* **2006**, *71*, 861–872. [[CrossRef](#)] [[PubMed](#)]
7. Bolm, C.; Schlingloff, G.; Weickhardt, K. Optically active lactones from a Baeyer-Villiger-type metal-catalyzed oxidation with molecular oxygen. *Angew. Chem. Int. Ed.* **1994**, *33*, 1848–1849. [[CrossRef](#)]
8. Arends, I.W.C.E.; Sheldon, R.A.; Wallau, M.; Schuchardt, U. Oxidative transformations of organic compounds mediated by redox molecular sieves. *Angew. Chem. Int. Ed.* **1997**, *36*, 1144–1163. [[CrossRef](#)]
9. Uyanik, M.; Ishihara, K. Baeyer-Villiger oxidation using hydrogen peroxide. *ACS Catal.* **2013**, *3*, 513–520. [[CrossRef](#)]
10. Jacobson, S.E.; Tang, R.; Mares, F. Oxidation of cyclic ketones by hydrogen peroxide catalysed by group 6 metal peroxo complexes. *J. Chem. Soc. Chem. Commun.* **1978**, 888–889. [[CrossRef](#)]
11. Phillips, A.M.F.; Romão, C. Synthesis of γ -butyrolactones by a Baeyer-Villiger oxidation with hydrogen peroxide, catalysed by methyltrioxorhenium. *Eur. J. Org. Chem.* **1999**, *1999*, 1767–1770. [[CrossRef](#)]
12. Fürst, M.J.L.J.; Gran-Scheuch, A.; Aalbers, F.S.; Fraaije, M.W. Baeyer-Villiger monooxygenases: Tunable oxidative biocatalysts. *ACS Catal.* **2019**, *9*, 11207–11241. [[CrossRef](#)]
13. Liu, C.-H.; Wang, Z.; Xiao, L.-Y.; Mukadas, Zhu, D.-S.; Zhao, Y.-L. Acid/Base-co-catalyzed formal Baeyer-Villiger oxidation reaction of ketones: Using molecular oxygen as the oxidant. *Org. Lett.* **2018**, *20*, 4862–4866. [[CrossRef](#)] [[PubMed](#)]

14. Tsang, A.S.-K.; Kapat, A.; Schoenebeck, F. Factors that control C-C cleavage versus C-H bond hydroxylation in copper-catalyzed oxidations of ketones with O₂. *J. Am. Chem. Soc.* **2016**, *138*, 518–526. [[CrossRef](#)]
15. van Beek, H.L.; Romero, E.; Fraaije, M.W. Engineering cyclohexanone monooxygenase for the production of methyl propanoate. *ACS Chem. Biol.* **2017**, *12*, 291–299. [[CrossRef](#)] [[PubMed](#)]
16. Bhaumik, A.; Kumar, P.; Kumar, R. Baeyer-Villiger rearrangement catalysed by titanium silicate molecular sieve (TS-1)/H₂O₂ system. *Catal. Lett.* **1996**, *40*, 47–50. [[CrossRef](#)]
17. Corma, A.; Nemeth, L.T.; Renz, M.; Valencia, S. Sn-zeolite beta as a heterogeneous chemoselective catalyst for Baeyer-Villiger oxidations. *Nature* **2001**, *412*, 423–425. [[CrossRef](#)]
18. Huang, H.-H.; Lu, M.-C.; Chen, J.-N. Catalytic decomposition of hydrogen peroxide and 2-chlorophenol with iron oxides. *Wat. Res.* **2001**, *35*, 2291–2299. [[CrossRef](#)]
19. Li, P.; Liu, G.; Wu, H.; Liu, Y.; Jiang, J.-G.; Wu, P. Postsynthesis and selective oxidation properties of nanosized Sn-beta zeolite. *J. Phys. Chem. C* **2011**, *115*, 3663–3670. [[CrossRef](#)]
20. Kang, Z.; Zhang, X.; Liu, H.; Qiu, J.; Yeung, K.L. A rapid synthesis route for Sn-beta zeolites by steam-assisted conversion and their catalytic performance in Baeyer-Villiger oxidation. *Chem. Eng. J.* **2013**, *218*, 425–432. [[CrossRef](#)]
21. Chang, C.C.; Cho, H.J.; Wang, Z.; Wang, X.; Fan, W. Fluoride-free synthesis of a Sn-BEA catalyst by dry gel conversion. *Green Chem.* **2015**, *17*, 2943–2951. [[CrossRef](#)]
22. Oumi, Y.; Takahashi, J.; Takeshima, K.; Jon, H.; Sano, T. Realumination of zeolite Y under acidic conditions. *J. Porous Mater.* **2007**, *14*, 19–26. [[CrossRef](#)]
23. Zhu, Z.; Xu, H.; Jiang, J.; Liu, X.; Ding, J.; Wu, P. Postsynthesis of FAU-type stannosilicate as efficient heterogeneous catalyst for Baeyer-Villiger oxidation. *Appl. Catal. A* **2016**, *519*, 155–164. [[CrossRef](#)]
24. González-Núñez, M.E.; Mello, R.; Olmos, A.; Asensio, G. Baeyer-Villiger oxidation in supercritical CO₂ with potassium peroxomonosulfate supported on acidic silica gel. *J. Org. Chem.* **2006**, *71*, 6432–6436. [[CrossRef](#)] [[PubMed](#)]
25. Zhu, Z.; Xu, H.; Jiang, J.; Wu, P. Postsynthesis and effective Baeyer-Villiger oxidation properties of hierarchical FAU-type stannosilicate. *J. Phys. Chem. C* **2016**, *120*, 23613–23624. [[CrossRef](#)]
26. Li, Q.; Zhang, Z.; Zhao, J.; Li, A. Recent advances in the sustainable production of α,ω -C6 bifunctional compounds enabled by chemo-/biocatalysts. *Green Chem.* **2022**, *24*, 4270–4303. [[CrossRef](#)]
27. Williams, C.K. Synthesis of functionalized biodegradable polyesters. *Chem. Soc. Rev.* **2007**, *36*, 1573–1580. [[CrossRef](#)] [[PubMed](#)]
28. Pyo, S.-H.; Park, J.H.; Srebny, V.; Hatti-Kaul, R. A sustainable synthetic route for biobased 6-hydroxyhexanoic acid, adipic acid and ϵ -caprolactone by integrating bio- and chemical catalysis. *Green Chem.* **2020**, *22*, 4450–4455. [[CrossRef](#)]
29. Xia, C.; Ju, L.; Zhao, Y.; Xu, H.; Zhu, B.; Gao, F.; Lin, M.; Dai, Z.; Zou, X.; Shu, X. Heterogeneous oxidation of cyclohexanone catalyzed by TS-1: Combined experimental and DFT studies. *Chin. J. Catal.* **2015**, *36*, 845–854. [[CrossRef](#)]
30. Nabae, Y.; Rokubuichi, H.; Mikuni, M.; Kuang, Y.; Hayakawa, T.; Kakimoto, M. Catalysis by carbon materials for the aerobic Baeyer-Villiger oxidation in the presence of aldehydes. *ACS Catal.* **2013**, *3*, 230–236. [[CrossRef](#)]
31. Zhang, Y.; Cheng, Y.; Cai, H.; He, S.; Shan, Q.; Zhao, H.; Chen, Y.; Wang, B. Catalyst-free aerobic oxidation of aldehydes into acids in water under mild conditions. *Green Chem.* **2017**, *19*, 5708–5713. [[CrossRef](#)]
32. Imam, R.A.; Freund, H.; Guit, R.P.M.; Fellay, C.; Meier, R.J.; Sundmacher, K. Evaluation of different process concepts for the indirect hydration of cyclohexene to cyclohexanol. *Org. Process Res. Dev.* **2013**, *17*, 343–358. [[CrossRef](#)]
33. Ma, L.; Xu, L.; Jiang, H.; Yuan, X. Comparative research on three types of MIL-101(Cr)-SO₃H for esterification of cyclohexene with formic acid. *RSC Adv.* **2019**, *9*, 5692–5700. [[CrossRef](#)] [[PubMed](#)]
34. Liu, H.; Sun, J.; Hu, H.; Li, Y.; Hu, B.; Xu, B.; Choy, W.C.H. Antioxidation and energy-level alignment for improving efficiency and stability of hole transport layer-free and methylammonium-free tin-lead perovskite solar cells. *ACS Appl. Mater. Interfaces* **2021**, *13*, 45059–45067. [[CrossRef](#)]
35. Fan, L.; Guo, X.; Shen, L.; Yang, G.; Liu, S.; Tian, N.; Wang, Z.; Chen, L. Reduction depth dependent structural reversibility of Sn₃(PO₄)₂. *ACS Appl. Energy Mater.* **2018**, *1*, 129–133. [[CrossRef](#)]
36. Wang, H.; Gregorczyk, K.E.; Lee, S.B.; Rubloff, G.W.; Lin, C.-F. Li-containing organic thin film-structure of lithium propane dioxide via molecular layer deposition. *J. Phys. Chem. C* **2020**, *124*, 6830–6837. [[CrossRef](#)]
37. Sing, K.S.W.; Everett, D.H.; Haul, R.A.W.; Moscou, L.; Pierotti, R.A.; Rouquérol, J.; Siemieniewska, T. Reporting physisorption data for gas/solid systems with special reference to the determination of surface area and porosity. *Pure Appl. Chem.* **1985**, *57*, 603–619. [[CrossRef](#)]
38. Hiyoshi, N. Nanocrystalline sodalite: Preparation and application to epoxidation of 2-cyclohexen-1-one with hydrogen peroxide. *Appl. Catal. A Gen.* **2012**, *419–420*, 164–169. [[CrossRef](#)]
39. Zhan, H.; Yang, X.; Wang, C.; Chen, J.; Wen, Y.; Liang, C.; Greer, H.F.; Wu, M.; Zhou, W. Multiple nucleation and crystal growth of barium titanate. *Cryst. Growth Des.* **2012**, *12*, 1247–1253. [[CrossRef](#)]
40. Gao, Z.R.; Balestra, S.R.G.; Gómez-Hortigüela, L.; Li, J.; Márquez-Alvarez, C.; Cambor, M.A. Dication containing three aromatic ring structure-directs toward a chiral zeolite, spans three cavities, and effectively traps water. *Chem. Mater.* **2022**, *34*, 3197–3205. [[CrossRef](#)]
41. Li, L.; Li, Y.; Pang, D.; Liu, F.; Zheng, A.; Zhang, G.; Sun, Y. Highly asymmetric hetero-Diels-Alder reaction using helical silica-supported Mn(III)-salen catalysts. *Tetrahedron* **2015**, *71*, 8096–8103. [[CrossRef](#)]

42. Maity, S.; Ram, F.; Dhar, B.B. Phosphorous-Doped Graphitic Material as a Solid Acid Catalyst for Microwave-assisted synthesis of β -ketoenamines and Baeyer-Villiger oxidation. *ACS Omega* **2020**, *5*, 15962–15972. [[CrossRef](#)] [[PubMed](#)]
43. The Computational Model of Sn-Beta Zeolite Modified from the Beta Zeolite Framework. Available online: <http://www.iza-structure.org/databases/> (accessed on 1 July 2022).
44. Bukowski, B.C.; Bates, J.S.; Gounder, R.; Greely, J. First principles, microkinetic, and experimental analysis of Lewis acid site speciation during ethanol dehydration on Sn-Beta zeolite. *J. Catal.* **2018**, *365*, 261–276. [[CrossRef](#)]
45. Shibata, K.; Kiyoura, T.; Kitagawa, J.; Sumiyoshi, T.; Tanabe, K. Acidic properties of binary metal oxides. *Bull. Chem. Soc. Jpn.* **1973**, *46*, 2985–2988. [[CrossRef](#)]

Disclaimer/Publisher's Note: The statements, opinions and data contained in all publications are solely those of the individual author(s) and contributor(s) and not of MDPI and/or the editor(s). MDPI and/or the editor(s) disclaim responsibility for any injury to people or property resulting from any ideas, methods, instructions or products referred to in the content.